Single-Cell Imaging Maps Inflammatory Cell Subsets to Pulmonary Arterial Hypertension Vasculopathy

Selena Ferrian[1,6], Erin F. Mccaffrey[1#], Toshie Saito[2#], Aiqin Cao[2], Noah F. Greenwald[1], Mark R. Nicolls[3,4,5], Trevor Bruce[1], Roham T. Zamanian[3,4], Patricia Del Rosario[3,4]
Marlene Rabinovitch[2*], Michael Angelo[1*]

1. Department of Pathology, Stanford University, Stanford CA, 94305, USA
2. Department of Pediatrics, Division of Cardiology, Stanford University, Stanford CA, 94305, USA
3. Division of Pulmonary, Allergy, and Critical Care Medicine and
4. Vera Moulton Wall Center for Pulmonary Vascular Disease, Stanford CA, 94305, USA
5. Veterans Affairs Palo Alto Health Care System, Palo Alto CA, 94305, USA
6. Early Clinical Development, Genentech Inc., South San Francisco CA, 94080, USA

# These authors contributed equally
* Co-senior and corresponding authors: Michael Angelo (mangelo0@stanford.edu, Telephone: 919-451-5347); Marlene Rabinovitch (marlener@stanford.edu, Telephone: 650-723-6928; FAX: 650-723-6700)

ABSTRACT

Rationale: Experimental and clinical observations are advancing immunotherapies to clinical trial in pulmonary arterial hypertension (PAH). However, comprehensive mapping of the immune landscape in and around pulmonary arteries (PAs) in lung tissue is necessary to predict how immune cells might induce pulmonary vascular pathology. While more severe vascular pathology is reported in *BMPR2* mutant patients classified as hereditary (H)PAH, the relationship to specific immune cell subsets has not been established. Emerging high throughput approaches such as multiplexed ion beam imaging by time-of-flight (MIBI-TOF) that labels antibodies with mass elements enables the study of multiple cells and states of activation in the same tissue section.

Methods: We applied MIBI-TOF to compare PAs and surrounding tissue from unused donor lungs with PAH lungs that were diagnosed as idiopathic (IPAH) or HPAH.

Measurements: We measured the number and proximity of immune cells to vascular lesions and to each other. Immune cell subsets that tracked with vascular pathology were interrogated *ex vivo* for stimulation of pulmonary arterial smooth muscle cell (PASMC) proliferation.

Results: Massive immune infiltration in I/HPAH was observed with intramural infiltration linked to PA occlusive changes. The presence of CD11c+DCs expressing SAMHD1, TIM-3 and IDO-1 within immune enriched microenvironments and neutrophils were associated with greater immune activation in HPAH. CD11c-DC3s (mo-DC-like cells) were linked to inflamed endothelial cells and proliferating SMCs. Co-culture studies reinforced a causal relationship between neutrophil extracellular vesicles and mo-DCs in mediating PASMC proliferation.

Conclusions: These findings merit consideration in predicting and assessing the efficacy of immunotherapies for PAH.

Keywords: Pulmonary arterial hypertension; vascular remodeling; MIBI-TOF; dendritic cells; indoleamine 2, 3-dioxygenase 1 (IDO-1); neutrophils; monocyte-derived dendritic cells (mo-DCs); interferon gamma (IFN-γ); *BMPR2* mutation.

INTRODUCTION

Pulmonary arterial hypertension (PAH) has a poor prognosis, with a mortality rate of almost 40% over 5 years (1). Recent studies support the role of chronic inflammation and altered immunity in the pathogenesis of PAH (2,3). Monocyte and macrophage recruitment (4,5), infiltration of T- and B cells (2), loss (6) and dysfunction of regulatory T cells, (7) and increases in classical dendritic cells (cDCs) and monocyte-derived dendritic cells (mo-DCs) (8) in pulmonary artery (PA) and lung tissue, have been associated with initiation and exacerbation of PAH. Furthermore, elevation of circulating inflammatory cytokines and protease (2,9), tertiary lymphoid tissue adjacent to PAs (10), neutrophil extracellular traps in plexogenic lesions (PLs) (11), and activation of DCs (12) have been described.

As a result, recent immunotherapies have emerged in clinical trials, including neutrophil elastase inhibitors, B- and T-cell activation inhibitors, TGF-β antagonists, and anti-cytokine therapies (13). However, developing a successful immunotherapy to reverse PAH pathology requires a comprehensive understanding of the immune cell landscape, its microenvironmental complexities, and how communication with the vascular cells leads to the initiation and progression of disease. For example, specific immune cell subsets may distinguish *BMPR2* loss-of-function mutations in hereditary (H)PAH that leads to more severe vascular pathology (14,15), inflammation (16,17), and increased risk of death (18) when compared to idiopathic (I)PAH.

Previous studies of immune processes in PAH have been limited by the number of markers studied simultaneously in preserved tissue or by the loss of tissue architecture in analyses of desegregated lung biopsies (8,19,20). These limitations highlight a need for comprehensive profiling of participating cell types among diseased PAs. Our study used multiplexed ion beam imaging by time-of-flight (MIBI-TOF) (21) with a thirty-five-marker panel that included immune cell differentiation, activation, and tissue-specific markers to elucidate the relationship between the immune cell landscape and the smooth muscle cell (SMC) mass as well as the progressive occlusion of PAs judged by vessel score (22,23). We gained novel insights into the immune cell types involved in PAH, their activation state and localization, which revealed novel interplays between immune, vascular, and non-vascular cells. We established whether differences were related to the severity of lesions in HPAH, associated with *BMPR2* or a *SMAD9* mutation, versus IPAH. Thus, we provide the first comprehensive architectural map of PAH lung tissue, to directly relate multiple immune cell populations to PA lesions, and to link the more severe pathology of HPAH to specific immune cell subsets and novel immune spatial features.

Our findings identified three cell types involved in PAH pathogenesis and progression. We observed increased tolerogenic DCs in HPAH, preferentially distributed in immune activated microenvironments. The spatial arrangements of mo-DCs and neutrophils strongly associated with SMC mass and increased severity of lesions, with subsequent cell culture studies documenting the role of both cell types in SMC hyperplasia. Our findings suggest that these three cell types should be considered in the development of biomarkers and immunotherapies for PAH.

METHODS

An Expanded Methods section is available in the Online Data Supplement.

PAH patient and control samples. Lung tissues at the time of transplant from PAH and unused donor controls (Con) were provided by the Pulmonary Hypertension Breakthrough Initiative and the CMREF. Peripheral blood mononuclear cells (PBMCs) were isolated from PAH and donor control blood obtained from the Stanford biobank and the Stanford Blood Bank, respectively.

Histopathological Scoring. Approximately five representative PAs were selected per patient based on scoring of vascular morphology. See Figures 2A, and E1A in the Online Data Supplement.

Reagents. See Table E1 and Figure E1E-F in the Online Data Supplement.

Tissue staining and imaging. Tissue was stained with a 35-marker panel and imaged using MIBI-TOF as previously described (21). See Figures 1A-D and E1B in the Online Data Supplement.

Image Processing and Segmentation. Image processing and segmentation were carried out as previously described (21). See Figures 1D and E1C-D in the Online Data Supplement.

Cell Profiling and Functional Analysis. Single cell data were extracted as previously described (24). Cell phenotype maps were generated using the Bioconductor "FlowSOM" package (25). Positivity thresholds for functional proteins were conducted using the "MetaCyto" package (26). See Figure 1E-F.

Vascular Region Masking. Three vascular regions were generated using the α-SMA staining. An intramural region (IM) corresponding to α-SMA staining and a 'perivascular' region (PV) within 100 pixels of the vessel perimeter. Any region beyond that was considered 'non-vessel' (NV). See Figure 2B.

Spatial Analyses. The minimum distance for each cell to the vessel perimeter was calculated. Additionally, cell neighborhoods were produced by first generating a cell neighbor matrix, where each row represents an index cell, and the columns indicate the relative frequency of each cell phenotype within 50 pixels of the index cell. See Figure 5A and E5A in the Online Data Supplement.

Pulmonary arterial SMC isolation. PASMCs were harvested from explanted lungs of Con patients and cultured in SMC growth medium. See Figure 6D.

Exosome isolation from plasma and CD66b pulldown. Exosomes were isolated from plasma of Con patients using the Exosome Total Isolation Chip (ExoTIC). ExoTIC-harvested exosomes were further purified using Dynabeads conjugated to CD66b/CEACAM 8. See Figure 3G.

Monocyte Derived-Dendritic Cells Generation. Human CD14+cells from a Con and IPAH patients PBMC were obtained using human CD14 Microbeads and differentiated into mo-DCs (CellXVivo Human Monocyte-derived DC Differentiation Kit). See Figure 6D.

MTT Cell Proliferation Assay. PASMCs from a Con patient were incubated overnight followed by 48 hours starvation in 0.2% FBS SMC medium. Then PASMCs media were treated with optimal dose of neutrophil-derived exosomes (10,000 count/cell). PASMC proliferation was assessed by 3-(4,5-dimethylthiazol-2-yl)-2,5-diphenyltetrazolium bromide (MTT) assay after 72 hours of incubation.

Cell co-cultures. Mo-DCs and PASMCs were incubated in 0.2% FBS SMC medium for 72 hours in a 1:1 ratio. Following co-cultures, SMCs were lift by TrypLE express and counted (Scepter). See Figure 6D.

Statistical Analysis. Significance was determined by two-sided unpaired t-test, or by Kruskal-Wallis test followed by a Dunn's multiple comparison test. Repeated-measures one-way ANOVA with Tukey's multiple comparisons test was carried out for analyses among groups with repeated samples from the same individual in each group. Spearman' s rank correlations were carried out.

RESULTS

Mapping vascular lesions in pulmonary arterial hypertension

To understand the immune landscape related to PAH pathology, we curated de-identified fixed tissue sections from explanted lungs removed at the time of transplant from PAH patients (n=12) and unused donor lungs from controls (Con, n=10) (**Figure 1A**). Six PAH patients were classified as IPAH and six as HPAH. Demographic and clinical data closest to transplant are summarized in **Table 1**. A total of 90 PAs were evaluated and scored in relation to the severity of the lesion. MIBI-TOF revealed specific cell subsets related to vascular pathology, that were pursued in co-culture studies (**Figures 1A-B** and **E1A** in the Online Data Supplement).

For MIBI-TOF, thirty-five markers were used to identify non-immune and immune cells in addition to markers related to metabolism, antigen presentation, and immune regulation (**Figure 1C**; **Table E1** in the Online Data Supplement). Details related to image acquisition and processing, antibody titration and validation are given in **Figure E1B-F** in the Online Data Supplement. Regions of interest (ROIs) were selected based on H&E stain and imaged using MIBI-TOF (**Figure 1D**) to assess the composition of the immune infiltrate. FlowSOM clustering (25) was applied to generate cell phenotype maps (CPMs), where each cell is labeled by its phenotype (**Figure 1E**). The expression profiles and abundance of key lineage markers across all subsets are shown in **Figure 1F**.

Unrelated to their circulating counterparts, our results showed a massive infiltration of immune cells in PAH (**Figures 1G** and **E2A-B** in the Online Data Supplement), suggesting that recruited immune cells may proliferate or remain viable longer in the tissue. Scant Tregs were found across the PAH cohort. With the exception of NKs, each immune cell type was increased in PAH (**Figure 1H**). Further analyses revealed an increase not only in the number but in the proportion of B cells in PAH compared to Con lungs, partially related to the presence of tertiary lymphoid structures (TLSs) (**Figure E2C-D** in the Online Data Supplement).

Intramural immune cells relate to vascular pathology

To understand how the spatial localization of immune cells relates to vascular pathology, we used a scoring system of progressive PA occlusion (**Figure 2A**). Masks were also generated to define three regions related to the PA: intramural (IM), perivascular (PV) and nonvascular (NV) (**Figure 2B**). Although total cellularity and immune cell count were higher in PAH compared to Con patient tissue sections across all regions (**Figure E2E-F** in the Online Data Supplement), the

relative immune subset distribution remained constant across regions (**Figure E2G** in the Online Data Supplement). Since no correlation was found between the overall immune cell infiltration and vessel score (r=-0.049; p=0.747), we examined this association in the three vascular regions. **Figure 2C** highlights a positive correlation between vessel score and intramural immune cells, involving monocytes, DCs, macrophages, CD4 and CD8 T cells (**Figure 2D**).

Extracellular vesicles from neutrophils contribute to severe pathology in HPAH patients

We next addressed the extent to which the PAH vascular and immune cell subgroups could be driving the correlation with vascular pathology. A trend toward a higher vessel score was noted in the HPAH compared to IPAH group, along with a significant increase in SMC count indicating greater SMC hyperplasia (**Figures 3B** and **E3A** in the Online Data Supplement) (15).

We next investigated whether the nature and distribution of the immune cells correlated with SMC hyperplasia in HPAH vs. IPAH. Despite comparable numbers of immune cells (**Figure E3B** in the Online Data Supplement), T cells, DCs, and monocytes were observed in closer proximity to the PA perimeter in HPAH compared to IPAH patients (**Figure 3C**), and their proximity correlated with increased SMC (CD4 cell: r=-0.3120; p=0.0309; CD8 cell: r=-0.4347; p=0.0019; DC: r=-0.3964; p=0.0070; Mono: r=-0.4318; p=0.0022). Furthermore, neutrophils within the perivascular and nonvascular regions were increased in HPAH compared to IPAH patients and correlated with SMCs (**Figures 3D-E** and **E3C-E** in the Online Data Supplement) with representative images in **Figure 3F**.

Given our recent findings on the role of neutrophil-derived extracellular vesicles (EVs) in inducing pulmonary hypertension in mice (27) and the positive correlation between the neutrophils and SMCs, we cultured EVs from neutrophils with PASMCs harvested from Con lungs. We found that neutrophil-derived EVs promote PASMC proliferation (**Figure 3G**).

Tolerogenic DCs reflect greater immune activation in HPAH patients

In carrying out the MIBI-TOF analyses, we selected functional markers of immune cell activation, including IFN-γ, iNOS and Granzyme B, and others based upon our previous studies. For example, our group previously identified SAM domain and HD domain-containing protein 1 (SAMHD1), in response to expansion of retroviral elements in myeloid and endothelial cells (22). As key immunoregulatory components of innate myeloid cells, immune checkpoint proteins such as PD-1/PD-L1, TIM-3, and IDO-1 were also included (28,29). These checkpoints are therapeutic targets in oncology and may be similarly relevant in PAH. Most of the studied markers were increased in immune cells in PAH compared to Con patients (**Figure E4A** in the Online Data Supplement). All cell lineages displayed increased IDO-1+ cells in PAH. Additionally, PAH patients exhibited an elevated frequency of IFN-γ+ and SAMHD1+ mesenchymal and ECs, along with elevated Ki-67+ SMC and mesenchymal cells. It was not surprising to find increased MHC class I and II expressing cells for every cell lineage in the PAH group, since elevated IFN-γ+ cells were observed (30). The prevalence o the Hb scavenger-receptor CD163, PD-L1, IDO-1, SAMHD1 and TIM-3 positive DCs, suggested different DC subtypes related to vascular pathology

(**Figures 4A** and **E4B-C** in the Online Data Supplement). The co-expression of IDO-1, TIM-3, and SAMHD1 on DCs was increased in HPAH compared to IPAH and positively correlated with IFN-γ expressing CD4 T cells (**Figures 4B** and **E4D-E** in the Online Data Supplement). Although no correlation was found with vessel score, this cell phenotype was positively correlated with Ki-67+ DCs and pulmonary arterial systolic pressure (PAP systolic, **Figures 4C** and **E4F** in the Online Data Supplement). Among four DC subsets, the tolerogenic DC phenotype expressing IDO-1, TIM-3, and SAMHD1 driving this difference was attributed to CD11c+DC1s (**Figure 4D-E**).

Immune-vascular cell interaction drives vascular remodeling

To find additional immune cell subsets that either individually or in combination could be contributing to vascular pathology, we conducted a 'neighborhood analysis' (**Figure E5A** in the Online Data Supplement). **Figure 5A** denotes how cell types are translated to cell neighborhood (CN) clusters, where the clustered cell types represent areas within the tissue with similar cellular composition. The architecture of the pulmonary tissue revealed the presence of ten CN clusters, composed of different combinations and prevalence of cell types (**Figures 5B** and **E5B** in the Online Data Supplement). The tight interaction among several immune cells translated to CN2, a tissue region mainly enriched by CD4 T cells, macrophages, monocytes, and DCs, with an activated microenvironment (**Figures 5B** and **E5C** in the Online Data Supplement). SMCs were prevalent in CN4 and to a lesser extent in CN1, accompanied mainly by monocytes. Lymphoid cells and DCs tend to cluster into immune prevalent CNs (CN2, CN6 and CN10), while neutrophils and NK cells preferentially localized within immune (CN2) and endothelial (CN5 and CN8) CNs. The increased tolerogenic DCs and neutrophils in HPAH vs. IPAH patients, accumulated in immune prevalent (CN2, CN6) and endothelial enriched (CN8) cell neighborhoods, respectively (**Figure E5D-E** in the Online Data Supplement).

Among the CNs a positive correlation, mainly driven by the HPAH group, was found between the frequency of CN1 and CN4 and vessel score, with stronger correlation found for CN1 (**Figure 4C**). Immune cells including T cells, DCs, monocytes, and macrophages in both CNs, along with endothelial and mesenchymal cells within CN1 positively correlated with vessel score (**Figure 4D-E**). Interestingly, when these cells were localized within other CNs, no associations were found, suggesting that an interaction of immune cells with SMCs and ECs may drive the correlation with score. This prompted us to further investigate the functional profile of immune cells within CN1.

Mo-DC-like cells in CN1 drive vascular remodeling

CD11c-DC3s co-expressing CD163, CD209, and CD14, a monocyte-derived DC (mo-DC)-like subset, were prevalent within areas in close interaction with SMCs (CN1) and to a lesser extent in other neighborhoods (**Figure 6A-B**). However, only when found within CN1, was there a correlation with vessel score, inducible nitric oxide synthase (iNOS)+ ECs, and proliferating SMCs (**Figure 6C**), which prompted us to investigate their effect on SMC proliferation.

We therefore generated mo-DCs from PAH and control PBMC. Both mature and immature mo-DCs were co-cultured with PASMCs harvested from donor controls. PASMC-PASMC co-cultures were introduced as a control (**Figure 6D**). Both immature and mature mo-DCs, from PAH patients, triggered greater PASMC proliferation compared to mo-DC from controls (**Figure 6E**), establishing a role for this subset in vascular remodeling.

Our working model is summarized in **Figure 6F**. The interaction and location of immune cells in PA tissue can impact vascular pathology. (**a**) Progressive vascular occlusion in PAH reflected in increased SMC mass and vessel area, and associated with (**b**) intramural T cells, monocytes, DCs and macrophages. (**c**) CD11c-DC3s (mo-DC-like cells) positively correlated with proliferating SMCs and inflamed ECs. Co-culture studies demonstrated a positive impact of mo-DCs on PASMC proliferation. Increased SMC mass and vessel area distinguished HPAH vs. IPAH better than vessel score, suggesting that the severity of occlusion may reflect one aspect of the pathology and SMC mass another or it may reflect differing sensitivities of these measurements. (**d**) Neutrophils in the perivascular and nonvascular regions were related to greater SMC mass in HPAH *vs.* IPAH. Co-culture studies supported the impact of remote neutrophil-derived EVs on SMC proliferation. Furthermore, HPAH tissues displayed increased immune activation compared to IPAH, judged by the (**e**) proximity of immune cells to the PAs, and the presence of tolerogenic CD11c+DC1s within immune enriched neighborhoods.

DISCUSSION

The PA wall is considered immunoprivileged (31). Prior studies focused on perivascular inflammatory cells (19,20,32) or cytokine profiles (33,34) associated with pulmonary arteriopathies. Our study showed a massive intramural immune infiltration that correlated with progressive PA occlusive score. This suggests that the breach of immunoprivilege serves as a propagator of vascular pathology. Except for NKs and Tregs, the remaining cell types were increased in PAH, as previously reported (19,20,35,36,37). Despite increased circulating Tregs (37,38), reduced FOXP3+ cells were reported in lung and PA tissue from IPAH patients compared to controls (19). Our analyses revealed scant Tregs among PAs in PAH suggesting a failure of Tregs to adequately control local immune activation, consistent with prior studies in athymic rats (6), which could represent a predisposing factor for the development of disease. In PAH, recruited immune cells can directly contribute to vascular remodeling by sustained production of pro-inflammatory factors (2). Our study adds to this paradigm by showing increased MHC class I and II positive cells in both ECs and α-SMA+ vascular cells, suggesting a positive feedback loop that propagates intramural inflammation.

BMPR2 loss-of-function mutations lead to more severe disease and increased risk of death in PAH (18). In addition to increased PA muscularization (14,15), clinical and experimental studies have linked reduced expression of *BMPR2* with inflammation (16,17). Loss of *BMPR2* promotes recruitment of immune cells, including monocytes (39), macrophages (5) and neutrophils

(17) into the lungs, exacerbating PAH. In addition to the proximity of different immune cells to the vessel perimeter, HPAH patients displayed increased neutrophils compared to IPAH and controls. Their extramural localization correlated with SMC mass, likewise, increased in HPAH. Elevated circulating levels of neutrophils have been reported in PAH compared to control patients (9,27,40). Neutrophils may cause PAH through different mechanisms, namely by releasing neutrophil elastase (27) and myeloperoxidase, a catalyst for reactive oxygen species (ROS) formation (41). Our functional studies indicate that neutrophil-derived EVs, that are enriched in elastase (27) promote SMC proliferation, consistent with a mechanism previously demonstrated on elastase release of growth factors (23).

Consistent with elevated levels of endogenous retroviral elements in macrophages from PAH patients (22) that could invoke an IFN-γ response, aberrant IFN-γ+ cells were observed in PAH compared to controls. IFN-γ is known to play a role in DC switching to a tolerogenic phenotype by inducing IDO-1 expression (42). Our study identified a DC subtype, named CD11c+DC1s, expressing IDO-1, SAMHD1 and TIM-3 that were increased in HPAH compared to IPAH. These cells appear to represent a tolerogenic DC subtype involved in immune suppression, as shown in rodent models of autoimmune diseases (43). Thus, their proliferative nature and correlation with IFNγ-producing CD4 T cells and PAP systolic, suggests a state of heightened inflammation in HPAH patients (17), as tolerogenic DCs proliferate to restore immune homeostasis.

Different DC subsets appear to provide differential cues controlling the process of inflammation and vascular remodeling (10,44). A subset of DCs expressing CD14, CD209, MHC class II and CD163 (mo-DCs-like cells), was closely aligned with vascular remodeling. Although the scavenger receptor CD163 is considered an M2 macrophage phenotype marker, its expression has been reported on monocytes and mo-DCs (45). scRNA-seq analysis of CD163+ monocytes demonstrated that they have an inflammatory M1-like signature (46). At the site of inflammation, mo-DCs differentiate from monocytes in an IFN-γ dependent manner (47), supporting our observation of increased IFN-γ+ immune cells in PAH. Mo-DCs are inconspicuous in the steady state but become prominent during inflammation (47). Two types of inflammatory mo-DCs have been identified: TNFα- and iNOS-producing DCs (48) and their impact on T cells have been studied (44). These cells were identified in the adventitia of PAs of human and experimental PH and were correlated with lesion severity (32). In our study mo-DCs accumulated in proximity to PAH vascular cells and correlated with lesion severity. *In vitro* co-cultures of mo-DCs, particularly those generated from PAH patients, induced PASMC proliferation. Furthermore, their correlation with activated ECs suggests that sustained inflammation is an important trigger in PAH progression, by inducing and perpetrating EC dysfunction (49). Indeed, one of the first triggers for the development of PAH is thought to be EC injury in PAs (50). Collectively, we provide novel evidence that DC and neutrophil homeostasis is altered in a microenvironment dependent manner, in which cell interaction may impact their functional profile and their relationship to T cells and vascular cells.

A limitation of our study is that the lung tissues were taken from patients on vasodilator therapy with end-stage disease, thereby confounding signals derived from the primary pathogenesis and early molecular events. Nonetheless, these studies were able to elucidate the pathways by which immune cells, and in particular tolerogenic DCs, mo-DCs and neutrophils, play a key pathogenic role in PAH. Assessing changes in their expression and function merits consideration both as a biomarker and as a target of novel PAH immunotherapies.

Competing Interests

SF was a speaker for a webinar sponsored by IonPath Inc. MA has a patent related to the MIBI technology (US20150287578A1) and is board member, shareholder, and consultant in IonPath Inc. EFM have previously consulted for IonPath Inc.

Data and Code Repository

All custom code used to analyze data will be made available through a Github repository (https://github.com/angelolab) and all processed images and annotated single cell data will be made available in Mendeley's data repository.

Author Contributions

SF conceived the study design, performed experiments, acquired and processed the cohort data, conceptualized and implemented data analysis, and wrote the manuscript with MR. EFM developed the algorithms and assisted with data analysis. NFG assisted with cell segmentation. TS prepared the tissue microarray blocks after scanning the sections for the arteries and assisted with immunohistochemical staining. MR and TS provided histopathological scoring of pulmonary arteries. MN provided advice and critical review of the manuscript. AC performed functional assays. TB, assisted with antibody labeling. RZ and PR carried out the patient phenotyping. MA and MR supervised the work.

Sources Of Support

This work was supported by NIH-NHLBI grants P01 HL 108797 and R24 HL 123767 (MR). MA was supported by 1R01AG056287 and 1R01AG057915, 1U24CA224309, the Bill and Melinda Gates Foundation, and a Translational Research Award from the Stanford Cancer Institute. MR is also supported in part by the Dunlevie Chair in Pediatric Cardiology at Stanford University. EFM was supported by the NSF Graduate Research Fellowship (grant no. 2017242837). NFG was supported by NCI CA246880-01 and the Stanford Graduate Fellowship.

REFERENCES

1. Farber HW, Miller DP, Poms AD, Badesch DB, Frost AE, Muros-Le Rouzic E, et al. Five-year outcomes of patients enrolled in the REVEAL Registry. *Chest* 2015; 148: 1043-1054.
2. Rabinovitch M, Guignabert C, Humbert M, Nicolls MR. Inflammation and immunity in the pathogenesis of pulmonary arterial hypertension. *Circ Res* 2014; 115: 165-175.
3. Huertas A, Tu L, Humbert M, Guignabert C. Chronic inflammation within the vascular wall in pulmonary arterial hypertension: more than a spectator. *Cardiovasc Res* 2020; 116: 885-893.
4. Florentin J, Coppin E, Vasamsetti SB, Zhao J, Tai Y-Y, Tang Y, et al. Inflammatory macrophage expansion in pulmonary hypertension depends upon mobilization of blood-borne monocytes. *J Immunol* 2018; 200: 3612-3625.
5. Sawada H, Saito T, Nickel NP, Alastalo T-P, Glotzbach JP, Chan R, et al. Reduced BMPR2 expression induces GM-CSF translation and macrophage recruitment in humans and mice to exacerbate pulmonary hypertension. *J Exp Med* 2014; 211: 263-280.
6. Tamosiuniene R, Tian W, Dhillon G, Wang L, Sung YK, Gera L, et al. Regulatory T cells limit vascular endothelial injury and prevent pulmonary hypertension. *Circ Res* 2011; 109: 867-879.
7. Huertas A, Phan C, Bordenave J, Tu L, Thuillet R, Le Hiress M, et al. Regulatory T cell dysfunction in idiopathic, heritable and connective tissue-associated Pulmonary Arterial Hypertension. *Chest* 2016; **149**: 1482-1493.
8. Marsh LM, Jandl K, Grünig G, Foris V, Bashir M, Ghanim B, et al. The inflammatory cell landscape in the lungs of patients with idiopathic pulmonary arterial hypertension. *Eur Respir J* 2018; 51.
9. Sweatt AJ, Miyagawa K, Rhodes CJ, Taylor S, Del Rosario PA, Hsi A, et al. Severe pulmonary arterial hypertension is characterized by increased neutrophil elastase and relative elafin deficiency. *Chest* 2021; 160: 1442-1458.
10. Perros F, Dorfmüller P, Montani D, Hammad H, Waelput W, Girerd B, et al. Pulmonary lymphoid neogenesis in idiopathic pulmonary arterial hypertension. *Am J Respir Crit Care Med* 2012; 185: 311-321.
11. Aldabbous L, Abdul-Salam V, McKinnon T, Duluc L, Pepke-Zaba J, Southwood M, et al. Neutrophil extracellular traps promote angiogenesis: evidence from vascular pathology in pulmonary hypertension. *Arterioscler Thromb Vasc Biol* 2016; 36: 2078-2087.
12. Koudstaal T, van Hulst JA, Das T, Neys SF, Merkus D, Bergen IM, et al. DNGR1-Cre–mediated deletion of Tnfaip3/A20 in conventional dendritic cells induces pulmonary hypertension in mice. *Am J Respir Cell Mol Biol* 2020; 63: 665-680.
13. Zolty R. Novel experimental therapies for treatment of pulmonary arterial hypertension. *J Exp Pharmacol* 2021; 13: 817.

14. Zhang S, Fantozzi I, Tigno DD, Yi ES, Platoshyn O, Thistlethwaite PA, et al. Bone morphogenetic proteins induce apoptosis in human pulmonary vascular smooth muscle cells. *Am J Physiol Lung Cell Mol Physiol* 2003; 285: L740-L754.
15. Morrell NW, Yang X, Upton PD, Jourdan KB, Morgan N, Sheares KK, et al. Altered growth responses of pulmonary artery smooth muscle cells from patients with primary pulmonary hypertension to transforming growth factor-β1 and bone morphogenetic proteins. *Circulation* 2001; 104: 790-795.
16. Hagen M, Fagan K, Steudel W, Carr M, Lane K, Rodman DM, et al. Interaction of interleukin-6 and the BMP pathway in pulmonary smooth muscle. *Am J Physiol Lung Cell Mol Physiol* 2007; 292: L1473-L1479.
17. Burton VJ, Ciuclan LI, Holmes AM, Rodman DM, Walker C, Budd DC. Bone morphogenetic protein receptor II regulates pulmonary artery endothelial cell barrier function. *Blood* 2011; 117: 333-341.
18. Evans JD, Girerd B, Montani D, Wang X-J, Galiè N, Austin ED, et al. BMPR2 mutations and survival in pulmonary arterial hypertension: an individual participant data meta-analysis. *Lancet Respir Med* 2016; 4: 129-137.
19. Savai R, Pullamsetti SS, Kolbe J, Bieniek E, Voswinckel R, Fink L, et al. Immune and inflammatory cell involvement in the pathology of idiopathic pulmonary arterial hypertension. *Am J Respir Crit Care Med* 2012; 186: 897-908.
20. Tuder RM, Groves B, Badesch DB, Voelkel NF. Exuberant endothelial cell growth and elements of inflammation are present in plexiform lesions of pulmonary hypertension. *Am J Pathol* 1994; 144: 275.
21. Keren L, Bosse M, Marquez D, Angoshtari R, Jain S, Varma S, et al. A structured tumor-immune microenvironment in triple negative breast cancer revealed by multiplexed ion beam imaging. *Cell* 2018; 174: 1373-1387. e1319.
22. Saito T, Miyagawa K, Chen S-Y, Tamosiuniene R, Wang L, Sharpe O, et al. Upregulation of human endogenous retrovirus-K is linked to immunity and inflammation in pulmonary arterial hypertension. *Circulation* 2017; 136: 1920-1935.
23. Taylor S, Dirir O, Zamanian RT, Rabinovitch M, Thompson A. The role of neutrophils and neutrophil elastase in pulmonary arterial hypertension. *Front Med* 2018; 5: 217.
24. McCaffrey EF, Donato M, Keren L, Chen Z, Delmastro A, Fitzpatrick M, et al. The immunoregulatory landscape of human tuberculosis granulomas. *Nat Immunol* 2022; 23: 318-329.
25. Van Gassen S, Callebaut B, Van Helden MJ, Lambrecht BN, Demeester P, Dhaene T, et al. FlowSOM: Using self-organizing maps for visualization and interpretation of cytometry data. *Cytometry A* 2015; 87: 636-645.
26. Hu Z, Jujjavarapu C, Hughey JJ, Andorf S, Lee HC, Gherardini PF, et al. MetaCyto: A tool for automated meta-analysis of mass and flow cytometry data. *Cell Rep* 2018; 24: 1377-1388.

27. Taylor S, Isobe S, Cao A, Contrepois K, Benayoun BA, Jiang L, et al. Endogenous retroviral elements generate pathologic neutrophils in pulmonary arterial hypertension. *Am J Respir Crit Care Med* doi:10.1164/rccm.202102-0446OC (2022).
28. Nakamura K, Smyth MJ. Myeloid immunosuppression and immune checkpoints in the tumor microenvironment. *Cell Mol Immunol* 2020; 17: 1-12.
29. Endo R, Nakamura T, Kawakami K, Sato Y, Harashima H. The silencing of indoleamine 2, 3-dioxygenase 1 (IDO1) in dendritic cells by siRNA-loaded lipid nanoparticles enhances cell-based cancer immunotherapy. *Sci Rep* 2019; 9: 1-11.
30. Stemme S, Fager G, Hansson G. MHC class II antigen expression in human vascular smooth muscle cells is induced by interferon-gamma and modulated by tumour necrosis factor and lymphotoxin. *Immunology* 1990; 69: 243.
31. Weyand CM, Goronzy JJ. Immune mechanisms in medium and large-vessel vasculitis. *Nat Rev Rheumatol* 2013; 9: 731-740.
32. Perros F, Dorfmüller P, Souza R, Durand-Gasselin I, Mussot S, Mazmanian M, et al. Dendritic cell recruitment in lesions of human and experimental pulmonary hypertension. *Eur Respir J* 2007; 29: 462-468.
33. Selimovic N, Bergh C, Andersson B, Sakiniene E, Carlsten H, Rundqvist B. Growth factors and interleukin-6 across the lung circulation in pulmonary hypertension. *Eur Respir J* 2009; 34: 662-668.
34. Soon E, Holmes AM, Treacy CM, Doughty NJ, Southgate L, Machado RD, et al. Elevated levels of inflammatory cytokines predict survival in idiopathic and familial pulmonary arterial hypertension. *Circulation* 2010; 122: 920-927.
35. Huertas A, Perros F, Tu L, Cohen-Kaminsky S, Montani D, Dorfmüller P, et al. Immune dysregulation and endothelial dysfunction in pulmonary arterial hypertension: a complex interplay. *Circulation* 2014; 129: 1332-1340.
36. Guignabert C, Tu L, Girerd B, Ricard N, Huertas A, Montani D, et al. New molecular targets of pulmonary vascular remodeling in pulmonary arterial hypertension: importance of endothelial communication. *Chest* 2015; 147: 529-537.
37. Austin E, Rock M, Mosse C, Vnencak-Jones C, Yoder S, Robbins I, et al. T lymphocyte subset abnormalities in the blood and lung in pulmonary arterial hypertension. *Respir Med* 2010; 104: 454-462.
38. Ulrich S, Nicolls MR, Taraseviciene L, Speich R, Voelkel N. Increased regulatory and decreased CD8+ cytotoxic T cells in the blood of patients with idiopathic pulmonary arterial hypertension. *Respiration* 2008; 75: 272-280.
39. Vengethasamy L, Hautefort A, Tielemans B, Belge C, Perros F, Verleden S, et al. BMPRII influences the response of pulmonary microvascular endothelial cells to inflammatory mediators. *Pflügers Arch* 2016; 468: 1969-1983.
40. Florentin J, Zhao J, Tai Y-Y, Vasamsetti SB, O'Neil SP, Kumar R, et al. Interleukin-6 mediates neutrophil mobilization from bone marrow in pulmonary hypertension. *Cell Mol Immunol* 2021; 18: 374-384.

41. Klinke A, Berghausen E, Friedrichs K, Molz S, Lau D, Remane L, et al. Myeloperoxidase aggravates pulmonary arterial hypertension by activation of vascular Rho-kinase. *JCI insight* 2018; 3.
42. Harden JL, Gu T, Kilinc MO, Rowswell-Turner RB, Virtuoso LP, Egilmez NK. Dichotomous effects of IFN-γ on dendritic cell function determine the extent of IL-12–driven antitumor T cell immunity. *J Immunol* 2011; 187: 126-132.
43. Stoop JN, Harry RA, von Delwig A, Isaacs JD, Robinson JH, Hilkens CM. Therapeutic effect of tolerogenic dendritic cells in established collagen-induced arthritis is associated with a reduction in Th17 responses. *Arthritis Rheum* 2010; 62: 3656-3665.
44. Van Uden D, Koudstaal T, van Hulst JA, Bergen IM, Gootjes C, Morrell NW, et al. Central role of dendritic cells in pulmonary arterial hypertension in human and mice. *Int J Mol Sci* 2021; 22: 1756.
45. Maniecki MB, Møller HJ, Moestrup SK, Møller BK. CD163 positive subsets of blood dendritic cells: the scavenging macrophage receptors CD163 and CD91 are coexpressed on human dendritic cells and monocytes. *Immunobiology* 2006; 211: 407-417.
46. Olaloye OO, Liu P, Toothaker JM, McCourt BT, McCourt CC, Xiao J, et al. CD16+CD163+ monocytes traffic to sites of inflammation during necrotizing enterocolitis in premature infants. *J Exp Med* 2021; 218: e20200344.
47. Shin KS, Jeon I, Kim BS, Kim IK, Park YJ, Koh CH, et al. Monocyte-derived dendritic cells dictate the memory differentiation of CD8+ T cells during acute infection. *Front Immunol* 2019; 10: 1887.
48. Serbina NV, Salazar-Mather TP, Biron CA, Kuziel WA, Pamer EG. TNF/iNOS-producing dendritic cells mediate innate immune defense against bacterial infection. *Immunity* 2003; 19: 59-70.
49. Parenti A, Pala L, Paccosi S, Rotella CM. Potential role for dendritic cells in endothelial dysfunction, diabetes and cardiovascular disease. *Curr Pharm Des* 2017; 23:1435-1444.
50. Ranchoux B, Harvey LD, Ayon RJ, Babicheva A, Bonnet S, Chan SY, et al. Endothelial dysfunction in pulmonary arterial hypertension: an evolving landscape (2017 Grover Conference Series). *Pulm Circ* 2018; 8: 2045893217752912.

FIGURE LEGENDS

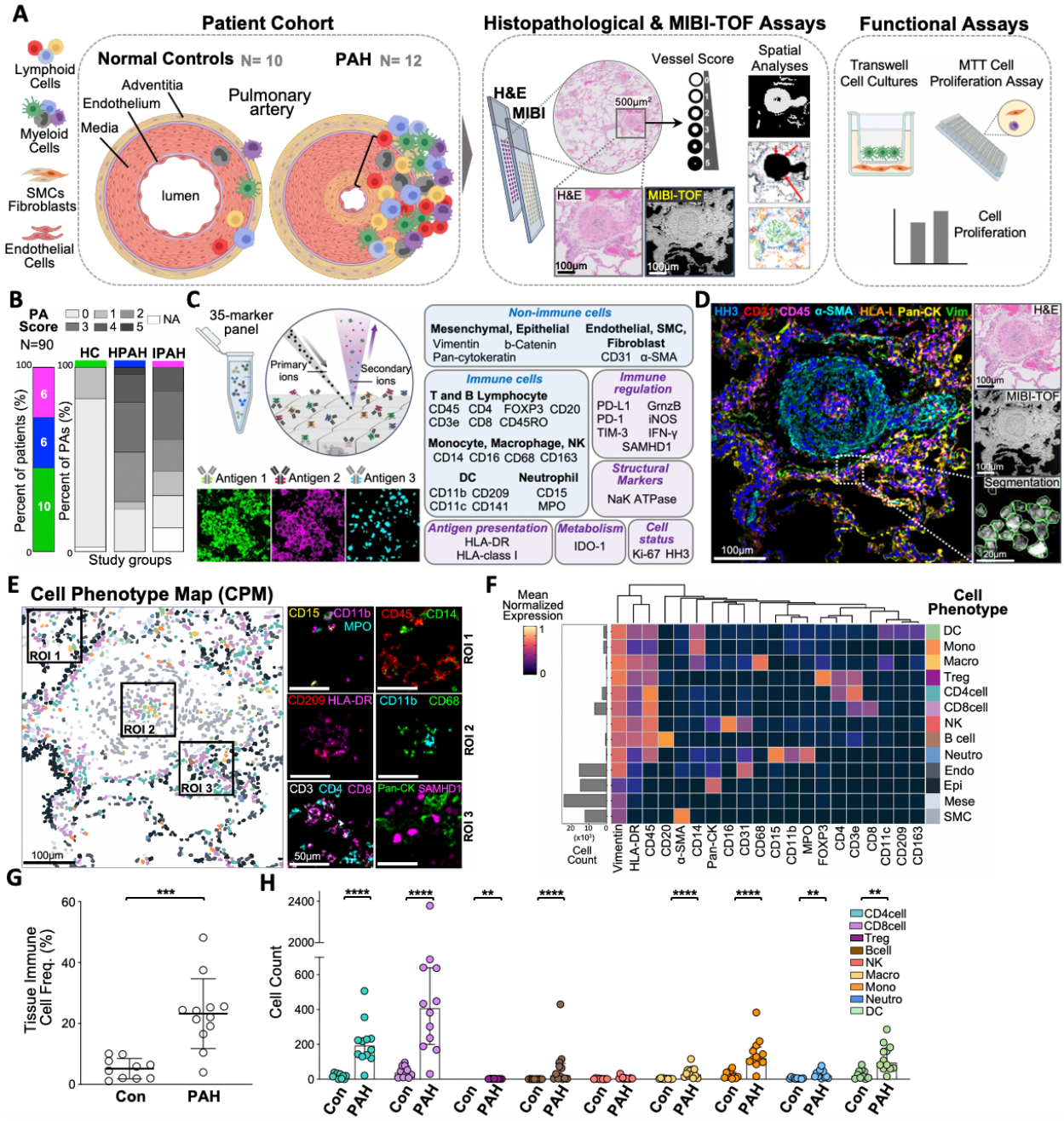

Figure 1. Multiplexed imaging interrogation of pulmonary arteries from pulmonary arterial hypertension patients and donor controls.

(A) Schematic depicting the workflow for the study. Representative pulmonary arteries (PAs) from ten donor control (Con) and twelve pulmonary arterial hypertension (PAH) patients were selected and embedded in a tissue microarray. PAs were scored on hematoxylin and eosin (H&E) in relation to the severity of the lesion and subsequent tissue sections were obtained to conduct MIBI-TOF analyses. Functional assays were carried out to confirm the MIBI-TOF findings. The PA images

were created using BioRender. **(B)** Stacked bar reporting the frequency of patients per study group, with the number of patients highlighted in white (left). The frequency of PA breakdown per vessel score across groups (right). Each region of interest imaged included a single PA scored from 0 to 5 according to the severity of the vascular pathology. NA was assigned to PAs for which score consensus was not reached or to representative regions of interest in the proximity but not adjacent to PAs. **(C)** Overview of the MIBI-TOF workflow and panel. Markers were grouped by target cell type or protein class. **(D)** Representative MIBI-TOF image overlay from a PA section along with the paired H&E, the carbon channel from imaging with MIBI-TOF and an image inset displaying the cell segmentation, scale bars = 100µm. (**E)** Cell phenotype map (CPM) overlay (left) showing cell identity by color, as defined in *F,* overlaid onto the segmentation mask, scale bar = 100µm. Six zoomed insets with adjacent MIBI-TOF overlays show diverse regions displaying neutrophil cells (ROI 1), DCs and macrophages (ROI 2), T cells along with epithelial and SAMHD1+ cells (ROI 3), scale bars = 50µm. **(F)** Cell lineage assignments based on mean normalized expression of lineage markers (heatmap columns) hierarchically clustered (Euclidean distance, average linkage). Rows are ordered by cell lineage (bottom) and immune cell breakdown (top). The absolute abundance of each cell type is displayed (left). (**G)** Frequency of immune cells (mean and SD) over total cells in donor controls (Con) and pulmonary arterial hypertension (PAH) patients. (**H)** Absolute count of immune cell subsets (median and IQR) in donor controls (Con) and pulmonary arterial hypertension (PAH) patients. α-SMA, alpha-smooth muscle actin; GrnzB, Granzyme B; MPO, myeloperoxidase; HLA-I, HLA-class I; Pan-CK, Pan-cytokeratin; HH3, histone H3; Vim, Vimentin; ROI, region of interest; Endo, endothelial cell; Epi, epithelial cell; Mese, mesenchymal cell; SMC, smooth muscle cell and fibroblast; DC, dendritic cell; Mono, monocyte; Macro, macrophage; Neutro, neutrophil; Treg, regulatory CD3+CD4+FOXP3+ cell; NK, natural killer (NK) cell; ROI, region of interest. All p-values were calculated with unpaired t test with Welch's correction or a Wilcoxon rank-sum test, where ns $p > 0.05$, *$p < 0.05$, **$p < 0.01$, ***$p < 0.001$, ****$p < 0.0001$.

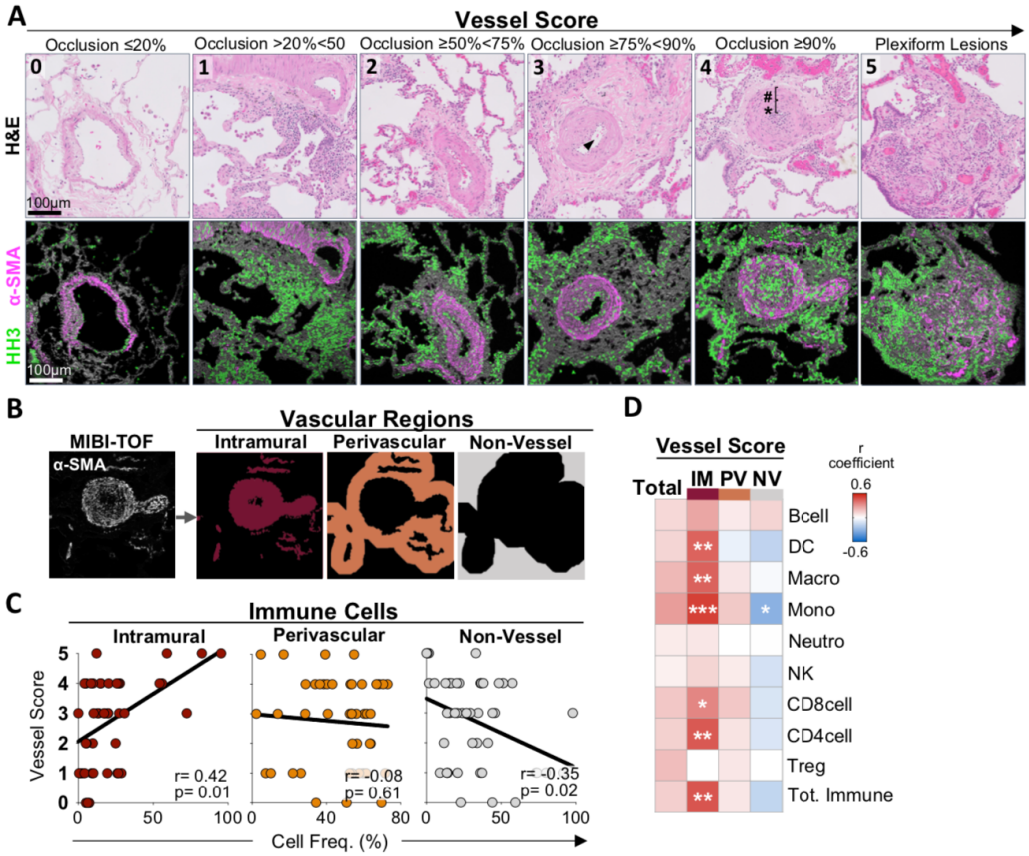

Figure 2. Intramural and extramural cell landscape of pulmonary arteries associated with progressive vascular pathology.

(A) Representative hematoxylin and eosin (H&E) images (top panel) of PAs from PAH patients scored from 0 to 5 according to the severity of the vascular pathology, characterized by medial hypertrophy (hash symbol), neointimal formation and fibrosis (asterix symbol) causing varying degrees of lumenal occlusion (arrow). See Methods section. Corresponding MIBI-TOF images overlay (bottom panel) displaying α-SMA (magenta), HH3 (green) and the carbon channel (grey). α-SMA marked both medial hypertrophy and neointimal formation, involving both smooth muscle cells and fibroblasts. Scale bars = 100µm. **(B)** Binary masks were generated to localize immune cells with respect to the vascular architecture. α-SMA staining from the MIBI-TOF scan was used to extrapolate the intramural region (maroon). A region within 100 px (~50 µm) of the vessel was defined as a 'perivascular' (dark orange). Any region beyond that was considered 'non-vessel' (grey). **(C)** The relationship between vessel score and the imm une cell distribution across vascular regions in PAH patients. **(D)** Heatmap displaying the relationship between immune cell counts across vascular regions (heatmap rows) and vessel score (heatmap columns). Heatmap includes total cell count (regardless of vascular region), Intramural (IM), Perivascular (PV), and Non-Vessel (NV) regions. The R correlation coefficient (black number) and the p-values (white asterix) are reported. Correlations were carried out using Spearman's rank correlation with 95% confidence interval and two-tailed test, where ns $p > 0.05$, *$p < 0.05$, **$p < 0.01$, ***$p < 0.001$, ****$p <$

0.0001. α-SMA, alpha-smooth muscle actin; HH3, histone H3; DC, dendritic cell; Mono, monocyte; Macro, macrophage; Neutro, neutrophil; Treg, regulatory CD3+CD4+FOXP3+ cell, NK, natural killer (NK) cell.

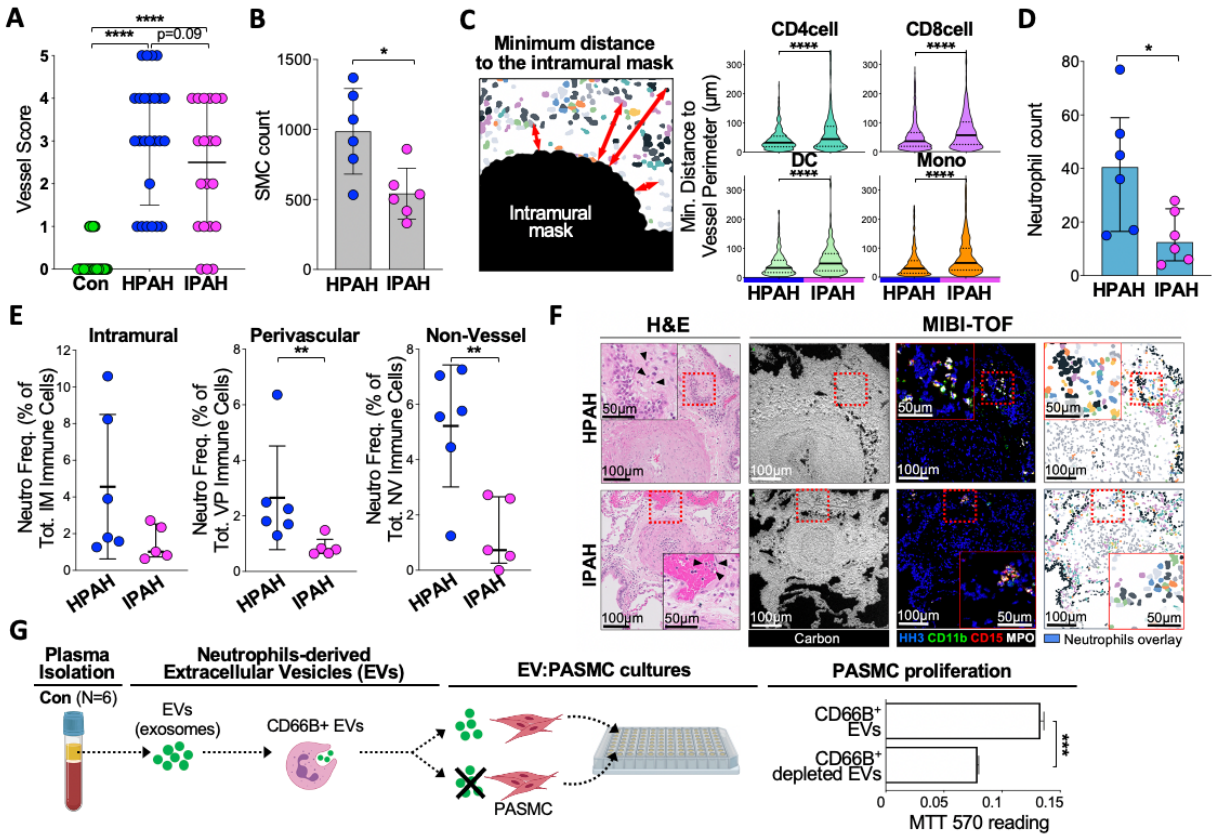

Figure 3. Spatial information of immune cell subsets drives differences observed between hereditary (H) and idiopathic (I) pulmonary arterial hypertension (PAH) patients.
(A) The vessel score (median and IQR) comparison across study groups. Green dots indicate donor control (Con) individuals, blue represent hereditary (HPAH) and magenta idiopathic (IPAH) pulmonary arterial hypertension patients. **(B)** Smooth muscle cell (SMC) count (median and IQR) overlaid with dot plots colored by PAH subgroups. **(C)** Schematic image depicting the minimum distance of extramural cell types to the intramural (IM) mask (left panel). Violin plots displaying the minimum distance (median, line; IQR, dotted lines) to the vessel perimeter of extramural immune cell subsets in PAH subgroups (right panel). **(D)** The neutrophil count (median and IQR) between PAH subgroups. **(E)** The frequency of neutrophil per vascular region between PAH subgroups. **(F)** Representative H&E and corresponding MIBI-TOF images of PAs from an HPAH (top panel) and IPAH (bottom panel) patient. The extramural presence of neutrophils is highlighted in the H&E zoomed insets (black arrows). The carbon channel from the MIBI-TOF scans reveals the structural similarity with the adjacent H&E section, followed by an overlay of MIBI-TOF channels to identify neutrophils (CD11b, CD15, MPO) along with a nuclei marker. Cell phenotype map from MIBI-TOF images displaying the neutrophils in blue. Images scale bars = 100µm; zoomed insets scale bars = 50µm. MPO, myeloperoxidase. **(G)** Workflow depicting the isolation of extracellular vesicles (EV) from neutrophils and co-culture with pulmonary arterial smooth muscle cells (PASMCs). EVs were isolated from six donor control plasma and purified using CD66b/CEACAM 8 antibody, while PASMCs were obtained from donor controls lung tissue. Bar

plot displaying the PASMC proliferation (median and IQR) in presence or absence of EVs derived from neutrophils. All p-values were calculated with a Wilcoxon rank-sum test or unpaired t test with Welch's correction, where ns $p > 0.05$, *$p < 0.05$, **$p < 0.01$, ***$p < 0.001$, ****$p < 0.0001$.

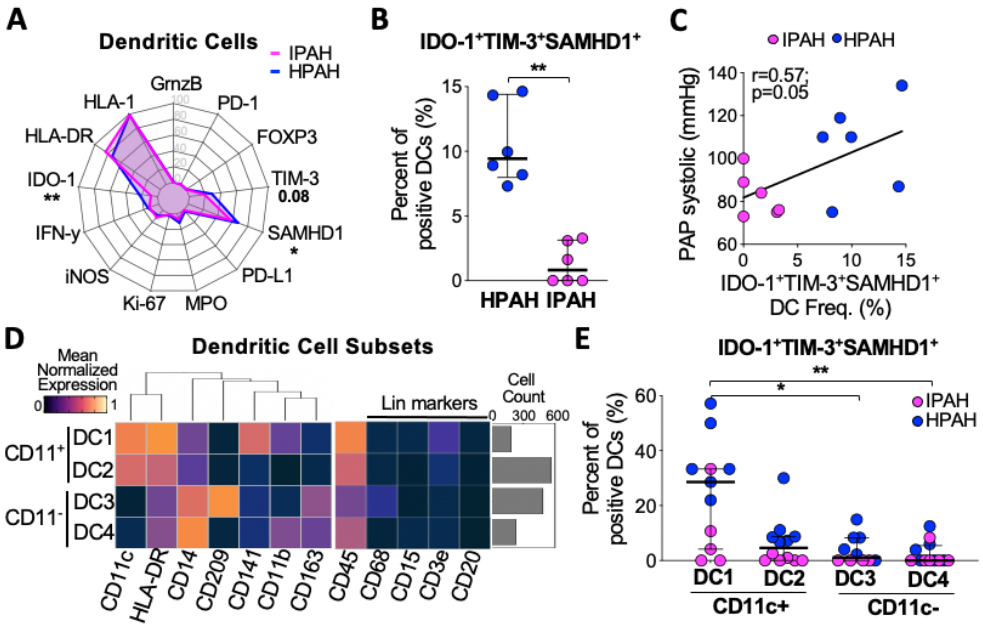

Figure 4. Tolerogenic DCs distinguishes hereditary (HPAH) from idiopathic (IPAH) pulmonary arterial hypertension patients and relates to their hemodynamic parameters. **(A)** Radar chart displaying the difference in functional marker expression between HPAH (blue line) and IPAH (magenta line) patients for dendritic cells. The median frequency of positive cells per marker and study group is displayed. **(B)** The frequency of dendritic cells (median and IQR) co-expressing IDO-1, TIM-3 and SAMHD1 in PAH subgroups. **(C)** The relationship between systolic pulmonary artery pressure (PAP systolic) and the frequency of DCs co-expressing IDO-1, TIM-3 and SAMHD1 in PAH patients. **(D)** Dendritic cell assignments based on mean normalized expression of phenotypic markers (heatmap rows) hierarchically clustered (Euclidean distance, average linkage). The absolute abundance of each cell type is displayed (right). Lin, Lineage. **(E)** Frequency of IDO-1+TIM-3+SAMHD1+ cells (median and IQR) across DC subsets in PAH patients. All p-values were calculated with a Kruskal-Wallis test followed by a Dunn's multiple comparison test, where ns $p > 0.05$, *$p < 0.05$, **$p < 0.01$, ***$p < 0.001$, ****$p < 0.0001$. All p-values were calculated with a Wilcoxon rank-sum test, where ns $p > 0.05$, *$p < 0.05$, **$p < 0.01$, ***$p < 0.001$, ****$p < 0.0001$. GrnzB, Granzyme B; MPO, myeloperoxidase; HLA-I, human leukocyte antigen class I; DC, dendritic cell; Mono, monocyte; Macro, macrophage; Neutro, neutrophil; NK, natural killer (NK) cell.

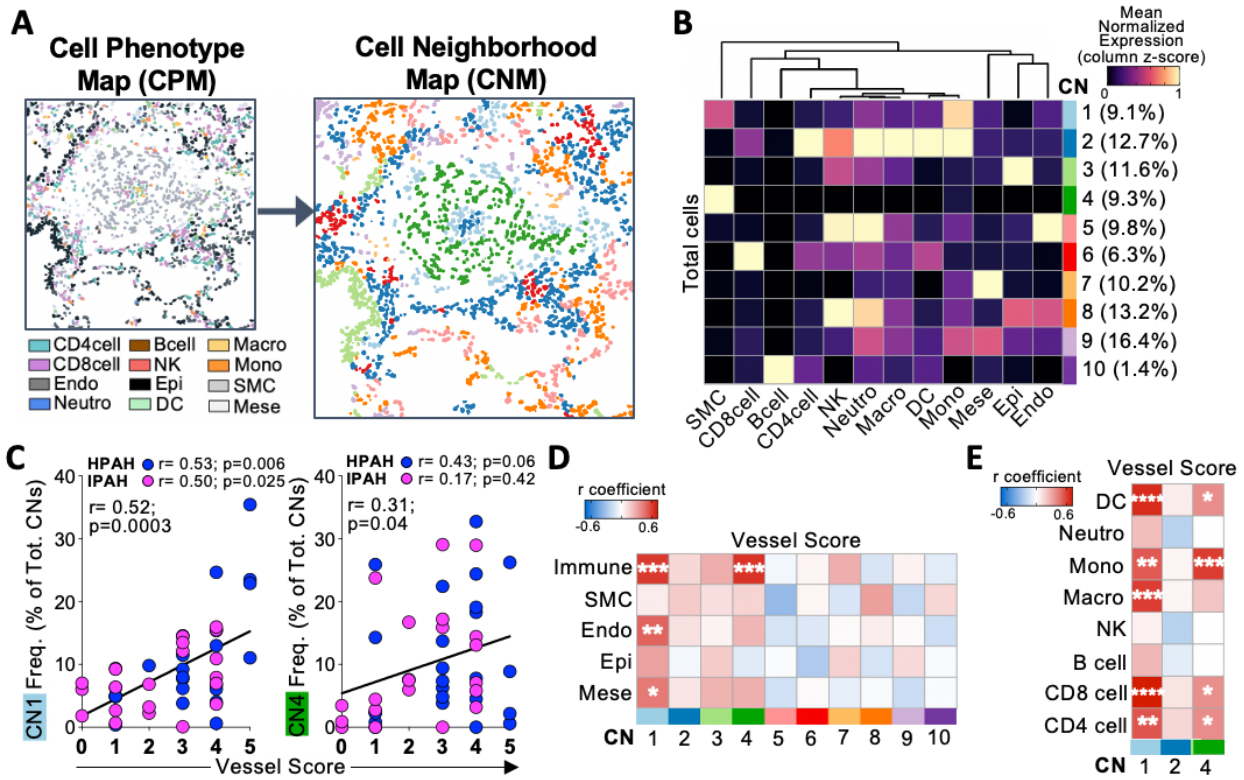

Figure 5. Neighborhood organization of immune cells in pulmonary arterial hypertension patients correlates with vascular remodeling.

(A) Representative Cell Phenotype Map (CPM) from a PAH patient displaying how cell types are grouped into a cell neighborhoods map (CNM). **(B)** Heatmap showing the mean normalized cell type frequency for each cell neighborhood (CN) (heatmap rows) hierarchically clustered (Euclidean distance, average linkage). Columns represent the cell types present in PAs. Ten CNs were identified: immune and smooth muscle cell-enriched (CN1), immune-enriched (CN2), epithelial-associated (CN3), smooth muscle cell-associated (CN4), immune and endothelial-enriched (CN5), T cell and DC-enriched (CN6), mesenchymal associated (CN7), immune and epithelial/endothelial-enriched (CN8), immune and mesenchymal-enriched (CN9), B cell-enriched (CN10) cell neighborhoods. **(C)** The relationship between vessel score and the frequency of CN1 and CN4, respectively, across PAH patients. Blue dots indicate hereditary (H)PAH, while magenta points represent idiopathic (I)PAH patients. The overall correlation is reported, with the breakdown for the HPAH and IPAH patients given below. **(D)** Heatmap displaying the correlation between the frequency of cell lineages within each cell neighborhood (CN, heatmap columns) and vessel score (heatmap rows). The R correlation coefficient (black number) and the p-values (white asterix) are reported. **(E)** Heatmap displaying the correlation between the frequency of immune cell subsets within CNs (heatmap rows) and vessel score (heatmap columns). The R correlation coefficient (black number) and the p-values (white asterix) are reported. All p-values were calculated with a Wilcoxon rank-sum test. All correlations were carried out using Spearman's rank correlation with 95% confidence interval and two-tailed test, where ns $p > 0.05$, *$p < 0.05$, **$p <$

0.01, ***$p < 0.001$, ****$p < 0.0001$. DC, dendritic cell; Mono, monocyte; Macro, macrophage; Neutro, neutrophil; NK, natural killer (NK) cell; Mese, mesenchymal cell; Epi, epithelial cell; SMC, smooth muscle cells and fibroblasts; Endo, endothelial cell; GrnzB, Granzyme B; HLA-class I, human leukocyte antigen class I; HLA-DR, human leukocyte antigen – DR isotype.

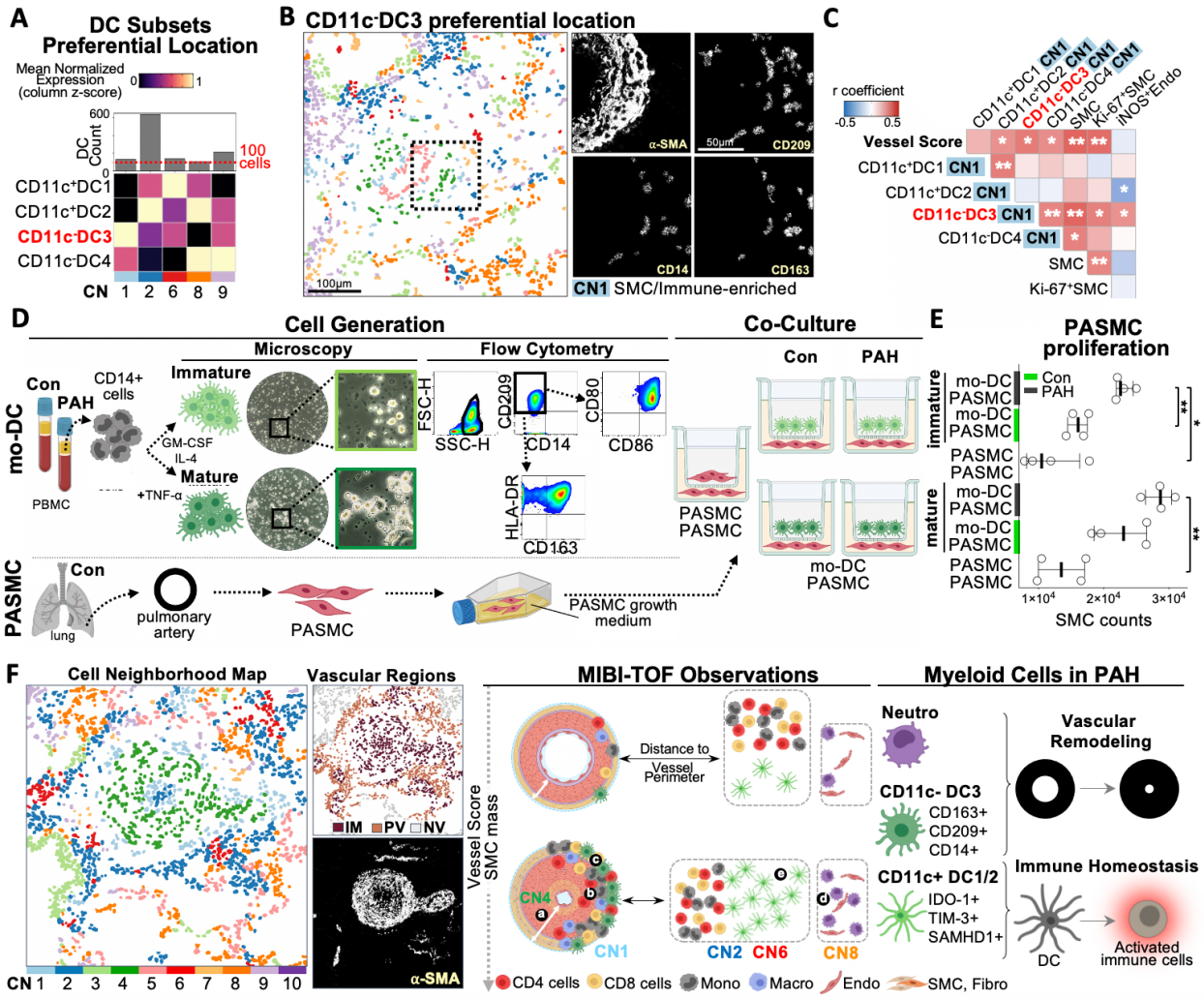

Figure 6. The spatial location of monocyte-derived dendritic cells dictates their involvement in smooth muscle cell proliferation and vascular remodeling.

(A) Heatmap showing the mean normalized frequency of DC subsets across cell neighborhoods (CNs) (heatmap rows). The absolute abundance of each cell type is displayed (top). Dotted red line represents the threshold for 100 cells. The CD11c-DC3s (mo-DC-like cells) highlighted in red, were the predominant DC subtype in CN1. **(B)** Representative Cell Phenotype Map (CPM) of a pulmonary artery showing the spatial localization of distinct neighborhoods (left panel), denoted by color as in *Fig. 5B*. A zoomed inset of a region including CN1 was chosen to examine the presence of CD11c-DC3s using CD14, CD209 and CD163 marker expression. α-SMA was displayed to highlight the pulmonary arterial tissue (right panel). CN map scale bar = 100μm; zoomed insets scale bars = 50μm. **(C)** Correlation plot displaying the association between DC subsets found within CN1, smooth muscle cells (SMCs), proliferating SMCs, iNOS-positive endothelial cells and vessel score. The R correlation coefficient (black number) and the p-values (white asterix) are reported. The CD11c-DC3s (mo-DC-like cells) are highlighted in red. **(D)** Schematic illustration depicting the workflow implemented to obtain and culture mo-DCs with SMCs from donor controls and PAH patients. Undifferentiated CD14+ cells were isolated from

peripheral blood mononuclear cells (PBMCs). CD14+ cells were incubated with differentiation media to obtain immature and mature mo-DCs. Light microscopy and flow cytometry were carried out to confirm the mo-DCs phenotype. Each mo-DC maturation stage was co-cultured with PASMCs in transwell at a ratio of 1:1. A separate well with only PASMCs served as a control. Side scatter height (SSC-H); forward scatter height (FSC-H). **(E)** Pulmonary arterial SMC (PASMC) proliferation (median and IQR) across co-culture conditions (immature mo-DC:PASMC; mature mo-DC:PASMC; PASMC:PASMC) and study groups (donor control and PAH patients). **(F)** Graphic summary of the results. All correlations were carried out using Spearman rank correlation with 95% confidence interval and two-tailed test. Repeated-measures one-way ANOVA with Tukey's multiple comparisons test was carried out for analyses among groups with repeated samples from the same individual in each group Comparisons between groups were calculated with a Wilcoxon rank-sum test, where ns $p > 0.05$, *$p < 0.05$, **$p < 0.01$, ***$p < 0.001$, ****$p < 0.0001$. PBMC, peripheral blood mononuclear cell; SMC, smooth muscle cell; Endo, endothelial cell; Fibro, fibroblast; DC, dendritic cell; Mono, monocyte; Macro, macrophage; Neutro, neutrophil; NK, natural killer (NK) cell; mo-DC, monocyte-derived DC.

TABLE LEGEND

Patient	Dx	Age-Gender	Ethnicity	Mutation	WBC (K/μL)	PAP Mean (mmHg)	PAP Systolic (mmHg)	Fick PVR (Wood Units)	6-Min Walk (m)	WHO Functional Class	Drug
PAH 1	HPAH	33-F	African American	BMPR2	6.3	48	75	15.57	326.1	NA	Sld, Ep(iv), Bs, Trp
PAH 2	HPAH	37-M	Caucasian	BMPR2	13.4	77	119	14.22	309	IV	Sld, Ep(iv), Stx, Am, Im, Trp(iv)
PAH 3	HPAH	27-F	Caucasian	BMPR2*	5.99	69	110	12.11	359.7	NA	Sld, Trp(iv), Trp(SC), Bs, Il
PAH 4	HPAH	33-F	Caucasian	BMPR2	16.91	48	87	9.74	288	II	Sld, Ep(iv), Bs, Trp(iv)
PAH 5	HPAH	56-F	Caucasian	-	10.14	75	110	NA	372.2	IV	Sld, Ep(iv), Bs, Am
PAH 6	IPAH	41-F	Caucasian	-	2	55	75	9.84	472.4	III	Sld, Ep(iv), Bs
PAH 7	IPAH	40-F	Caucasian	-	3.95	47	84	NA	294	III	Sld, Ep(iv), Am, Il
PAH 8	IPAH	49-F	Caucasian	-	2.56	75	100	16.76	326.1	IV	Sld, Ep(iv), Am
PAH 9	HPAH	25-F	Asian	SMAD9	7.5	87	134	20.96	201	III	Sld, Ep(iv), Bs
PAH 10	IPAH	55-F	African American	-	1.8	53	89	12.29	273.4	IV	Sld, Ep(iv), Bs
PAH 11	IPAH	24-M	Asian	-	4.99	48	73	9.56	356	III	Sld, Ep(iv), Bs, Am
PAH 12	IPAH	18-M	Asian	NA	5.9	67	76	NA	210	III	Sld, Ep(iv), Bs, Trp

Patient	Dx	Age-Gender	Ethnicity	Mutation	Cause of Death
Con 1	healthy	49-F	Caucasian	-	Intracranial Hemorrhage
Con 2	healthy	56-F	Caucasian	-	Cerebrovascular accident
Con 3	healthy	49-M	Caucasian	-	Stroke
Con 4	healthy	43-F	Caucasian	-	Cerebrovascular/Stroke
Con 5	healthy	55-F	Hispanic or Latino	-	Cerebrovascular/Stroke
Con 6	healthy	19-M	Caucasian	-	Anoxic brain injury
Con 7	healthy	47-F	Hispanic or Latino	-	Cerebrovascular/Stroke/Intracerebral hemorrhage
Con 8	healthy	54-M	Hispanic or Latino	-	Cerebrovascular/Stroke/Intracerebral hemorrhage
Con 9	healthy	34-F	Asian	-	Cerebrovascular/Stroke/Intracerebral hemorrhage
Con 10	healthy	46-F	Caucasian	-	Cerebrovascular/Stroke/Intracerebral hemorrhage

Table 1. Clinical and demographic characteristics of patients.

Clinical and demographic data were obtained from catheterization study performed closest to transplantation. [a]Dx; Diagnosis: Pulmonary arterial hypertension (PAH) classification: IPAH, Idiopathic PAH; HPAH, hereditary PAH, known mutation as stated. [b]PAP, pulmonary arterial pressure. [c]PVR, Pulmonary vascular resistance. Data were obtained from catheterization study performed closest to transplantation. [d]6-Min Walk = distance walked in six minutes. Data were obtained from study performed closest to transplantation. [e]WHO Functional Class Functional based on the symptoms when doing everyday activities (I-IV, IV severe). Data were obtained from study performed closest to transplantation. [f]PAH medications: Medications are listed according to total drug exposure during treatment period up to transplantation, not necessarily in combination. [*]Variant of unknown significance. Drugs abbreviations: Ep (Epoprostenol), Bs (Bosentan), Sld (Sildenafil), Trp (Treprostinil), Stx (Sitaxsentan), Am (Ambrisentan), Im (Imatinib), Il (Iloprost). iv (intravenous).